Dissolution and degradation of nuclear grade cationic exchange resin by Fenton oxidation combining experimental results and DFT calculations

Lejin Xu, Xiang Meng, Ming Li, Wuyang Li, Zengguang Sui, Jianlong Wang, Jun Yang

PII: S1385-8947(18)31886-2
DOI: https://doi.org/10.1016/j.cej.2018.09.169
Reference: CEJ 20008

To appear in: *Chemical Engineering Journal*

Received Date: 5 July 2018
Revised Date: 9 September 2018
Accepted Date: 21 September 2018

Please cite this article as: L. Xu, X. Meng, M. Li, W. Li, Z. Sui, J. Wang, J. Yang, Dissolution and degradation of nuclear grade cationic exchange resin by Fenton oxidation combining experimental results and DFT calculations, *Chemical Engineering Journal* (2018), doi: https://doi.org/10.1016/j.cej.2018.09.169

Dissolution and degradation of nuclear grade cationic exchange resin by Fenton oxidation combining experimental results and DFT calculations

Lejin Xu [a,b], Xiang Meng [a,b], Ming Li [a], Wuyang Li [a], Zengguang Sui [a], Jianlong Wang [c,d], Jun Yang [a,*]

[a] Department of Nuclear Engineering and Technology, School of Energy and Power Engineering, Huazhong University of Science and Technology, Wuhan 430074, P R China

[b] China-EU Institute for Clean and Renewable Energy, Huazhong University of Science and Technology, Wuhan 430074, P R China

[c] Institute of Nuclear and New Energy Technology, Key Laboratory of Advanced Reactor Engineering and Safety of Ministry of Education, Tsinghua University, Beijing 100084, P R China

[d] Beijing Key Laboratory of Radioactive Wastes Treatment, Tsinghua University, Beijing 100084, P R China

* Corresponding author

Tel.: +86 27 87540164

E-mail: yang_jun@hust.edu.cn; toyangjun@gmail.com (J. Yang)

Abstract

The Fenton oxidation of nuclear grade cationic exchange resin was investigated in view of the effects of initial temperature, H_2O_2 dosage, catalyst type and

concentration as well as initial pH. Initial temperature and H_2O_2 dosage exhibited a significant positive effect on the decomposition of cationic resins, whereas the initial pH showed a negative effect. Ferrous ions had higher catalytic ability than copper ions to the H_2O_2 activation for resin decomposition, and the best Fe^{2+} concentration was 0.3 M. Under the conditions of initial temperature of 75 °C, H_2O_2 dosage of 200 mL, Fe^{2+} concentration of 0.3 M and initial pH of 0.01, a weight reduction of 73% was achieved. The experimental results on Co-substituted mock samples indicated that the radionuclides loaded in the resins were concentrated in liquid residue. The decomposition of cationic resins followed the two-stage first-order kinetics that composed of a dissolution period of resin beads (first-stage) and a followed degradation stage of resin solution (second-stage). Combined with the UV-visible and infrared spectra and their corresponding density functional theory (DFT) calculations, the dissolution of resin beads was due to the desulfonation of the sulfonated aromatic rings and the oxidative fragmentation of the polymer backbone by hydroxyl radicals (•OH) formed in Fenton reactions. After the dissolution of resin beads, the oxidative degradation and mineralization process proceeded by the attack of •OH mainly in aqueous medium.

Keywords: Cationic resin; Fenton reagent; Two-stage; Kinetics; Mechanism

1. Introduction

Ion exchange resins (IERs) are extensively used for water treatment in different systems of the power plants including nuclear reactors. These resins, used for the

treatment of the water contaminated by radioactive ionic species, are classified as nuclear grade (NG) resins, which are manufactured by incorporating some special features (e.g. high exchange capacity and mechanical strength, wide applicability and versatility) [1, 2]. Spent resins are radioactive wastes, coming from various systems of the nuclear reactors, such as the primary and secondary cooling water, moderator water, spent fuel storage building water, etc. [1] These spent resins are loaded by radionuclides including uranium-235, uranium-238, strontium-90, cobalt-60 and caesium-137. Medium-level radioactive spent resins from a Chinese nuclear power plant were about 15 m^3/a for each nuclear power unit with the radioactive concentration of 3.7×10^5–3.7×10^{10} Bq/L containing 8% ^{60}Co, 27% ^{131}I, 55% ^{137}Cs and 10% other nuclides; low-level radioactive spent resins were about 10 m^3/a for each unit with the radioactive concentration of $<3.7 \times 10^5$ Bq/L containing <1% ^{60}Co, 27% ^{131}I, 72% ^{137}Cs and <1% other nuclides. These resins should be treated and disposed properly to minimize the potential hazard to the ecological environment and human health, and to maintain the sustainable development of the nuclear power.

For the treatment of radioactive spent resins, various technologies such as immobilization (e.g. cementation, vitrification, bituminization and plastic solidification), oxidative decomposition (including dry oxidation and wet oxidation), super compaction, high integrity container and microbial conversion treatment have been extensively studied [3]. Immobilization, especially direct cementation, is commonly applied to dispose spent resins, providing a more stable form. The spent

resins are physically encapsulated into cement-based solidification systems without any chemically bonding, and the cement and resins have not been solidified together [4]. Because the resin swells or shrinks when water is adsorbed or released, there is force and space existing between the dehydration resins and packing material, which leads to the decrease of mechanical strength of the final waste form and the leak of radioactive nuclides into contacting water [3-5]. Due to volume bulging and organic swelling problems, direct cementation requires several pretreatment procedures to reduce the amount of wastes. Dry oxidation, such as pyrolysis and incineration [6, 7], has a good performance on waste volume reduction, but harmful substances such as sulphuric or nitric oxides and additionally radionuclides may emit at high temperature. Wet oxidation has been developed to overcome these issues, such as acid digestion [8], Fenton oxidation [9-12], supercritical water oxidation [13-16], radio-sensitive photocatalysis [17], the hybrid process of Fenton dissolution followed by sonication and/or wet air oxidation [18, 19]. These techniques also have some disadvantages such as special requirements of container (especially for acid digestion), high temperature and pressure required in supercritical water oxidation, extra consumption of energy, high cost of treatment facility, etc. To date, there is still difficult in storage of radioactive waste from nuclear power plants, and there is no satisfactory industrial treatment for these wastes that needs additional studies.

Wet oxidation using the Fenton reagent has been proposed as an alternative method in destructing spent resins. Many fundamental and practical studies have been done on

resin decomposition by Fenton oxidation. The Oak Ridge National Laboratory (ORNL, Tennessee, USA) has used Fenton's reagent (H_2O_2 and Fe^{2+}) to destroy ion-exchange resins in radioactive waste tanks in laboratory-scale and pilot-scale tests [20]. The optimal reaction conditions were a dilute acidic solution (pH 3–5) and moderate temperatures (T 60–100 °C), and reaction products especially gaseous products were identified, such as carbon dioxide, carbon monoxide and trace quantities of volatile organics [20]. The Institute of Nuclear Energy Technology at Tsinghua University (INET, Beijing, China) has investigated the decomposition behavior of cationic, anionic, and mixed ion-exchange resins by H_2O_2–Ni^{2+}/Cu^{2+}, H_2O_2–Mn^{2+}/Cu^{2+}, H_2O_2–Fe^{2+}, H_2O_2–Cu^{2+}, and H_2O_2–Fe^{2+}/Cu^{2+} systems [21, 22]. The effects of temperature, amount of H_2O_2 and catalyst on reaction processes were studied, and the analytical results indicated that the radioactive nuclides were concentrated in decomposed solution and solid residues, and no radioactivity was detected in the off-gas [21, 22]. Zahorodna et al. [23, 24] have applied the optimal experimental design methodology to investigate the effects of reaction parameters on resin oxidation by Fenton process, i.e. Fe^{2+} and H_2O_2 concentrations and temperature, as well as to determine the optimal process parameter ranges. The photo-Fenton process was found to enhance the mineralization rate of resins, and the evolution of sulfate (SO_4^{2-}), CO_2, formic and oxalic acids was investigated to elucidate the oxidative mechanisms and differentiation between Fenton and photo-Fenton processes [24]. Our earlier studies have also evaluated the influencing factors on resin

degradation by Fenton and Fenton-like processes, such as temperature, type and concentration of catalysts, H_2O_2 dosage and pH value, and the possible degradation mechanisms of cationic resin and anionic resin were proposed [9, 10, 25]. Thus, most of these previous researches focus on examining the effects of reaction conditions. Few studies have examined the reaction kinetics of resin by oxidative processes. Gunale et al. [18, 19] have studied the hybrid processes for the degradation of IER, which were the Fenton process for the dissolution of IER followed by wet oxidation and/or sonication for the mineralization of IER. The kinetics of catalytic wet oxidation of the waste obtained after Fenton process was studied, showing that the mineralization reaction followed a two-step mechanism, viz. the fast oxidation of the organic substrate followed by a slower oxidation of low-molecular-weight compounds formed, such as acetic acid and oxalic acid [18, 19]. However, little attention has been paid to examining the kinetics of both dissolution and degradation of resins by Fenton process. Since the resin is a high polymer, the degradation mechanism is very complicated. Density functional theory (DFT) calculation can open up a new way for the exploration of degradation mechanism of refractory organic pollutants. The relevant decomposition mechanisms based on both experimental and simulation results have not been reported, which need to be further studied.

The spent resins generated from a nuclear power plant are usually present in a mixed or partially mixed form of cationic and anionic resins. The mixed resin can be analyzed (semi-quantitatively) using a FTIR based spectroscopic method [1], and

separated by a fluidized bed gravimetric separator utilizing their density difference [16]. Because of the difference in functional groups of cationic and anionic resins as well as the interaction of the corresponding byproducts, cationic resin was chosen as the target contaminant to better optimize the reaction conditions and to investigate the reaction mechanism in this work. The effects of reaction temperature, catalyst type and concentration, H_2O_2 dosage and solution pH on the dissolution and degradation of nuclear grade cationic resins were investigated. The corresponding reaction kinetics of dissolution stage and degradation stage were studied. The Fenton oxidation of cationic resins was also evaluated in view of the weight reduction of resins, the experimental results on Co-substituted mock samples, as well as the decomposition mechanism combining experimental results and DFT calculation.

2. Materials and methods

2.1. Resins and chemicals

The nuclear grade cationic resin (ZG C NR 50) used in this study is made by Zhejiang Zhengguang Industrial Co., Ltd., which has been applied in the primary loop of reactor in several nuclear power plants, the experimental reactors and the nuclear waste treatment plant in China. The characteristics and performance of the cationic resin are listed in Table 1. This NG cationic resin is a cross-linked styrene-divinylbenzene (ST-DVB) copolymer with the strong acid cation exchange site (e.g. $-SO_3^-H^+$) (Table 1).

Ferrous sulfate ($FeSO_4 \cdot 7H_2O$), copper sulfate ($CuSO_4 \cdot 5H_2O$), H_2O_2 (30%, wt%)

and NaOH were supplied by Sinopharm Chemical Reagent Co., Ltd. For the determination of chemical oxygen demand (COD) value of the oxidized resin solution, potassium dichromate ($K_2Cr_2O_7$), silver sulfate (Ag_2SO_4), sulfuric acid (H_2SO_4) and potassium hydrogen phthalate ($C_8H_5KO_4$) were obtained from Sinopharm Chemical Reagent Co., Ltd., and mercury sulfate ($HgSO_4$) was purchased from Guizhou Tongren Chemical Reagent Factory. All chemicals were of analytical grade and used without further purification, and second distilled water was employed in this study.

2.2. Experimental set-up and procedures

All experiments were conducted in a four-necked round-bottomed flask (500 mL) placed in a thermostatic water bath (LWB-24, LongYue Instrument Equipment Co., Ltd., Shanghai, China) with a mechanical stirrer, as depicted in Fig. 1. The speed of the stirrer was about 500 rpm. Twenty grams of cationic resins and 50 mL of catalyst solution ($FeSO_4 \cdot 7H_2O$ or $CuSO_4 \cdot 5H_2O$) were first added into the reactor. The pH value was adjusted by NaOH solution. The oxidative reactions were initiated by adding a desired dosage of H_2O_2 to the mixture of resins and catalyst solution, and 50 mL of catalyst solution was continued to be added into the reactor at a flow rate of 1 mL/min. Gases released were condensed during the operation, and the temperature of solution was recorded. Samples were taken at predetermined time intervals, and diluted for COD analysis. After 180 min, the reaction was stopped, and the weight of the residue was measured after dried in a vacuum oven at 80 °C for a week. Each

experiment was carried out at least in duplicate, and all results were expressed as a mean value.

Because Co and Cs are known as the primary radionuclides that can be substituted in spent cationic resins generated from nuclear power plants, non-radioactive Co-substituted mock samples were prepared to investigate the emission and distribution of Co during the Fenton oxidation of spent resins. Twenty grams of cationic resins were saturated by 0.5 M $CoCl_2 \cdot 6H_2O$.

The percentage of weight reduction was calculated according to the following formulation:

$$\text{Weight reduction (\%)} = (1 - w_t/w_0) \times 100\% \quad (1)$$

where w_0 is the weight of original dry resins, and w_t is the weight of dried residue after the reaction. It should be noted that the addition of the catalysts (and NaOH) was eliminated in the calculation.

2.3. Analytical methods

The dissolution and degradation of cationic resins was determined by measuring the increase and decrease of COD value of the resin solution with a standard dichromate method [26]. The measurement was carried out on a HACH DRB200 digestion and an A360 scanning UV/VIS spectrophotometer (AOE Instruments Co., Ltd., Shanghai, China). Test solutions (3 mL) were pipetted into a dichromate solution with concentrated sulfuric acid and digested at 165 °C for 15 min. The analyses of absorbance for the change in color of the dichromate solution were determined at the

wavelength of 440 nm.

The pH values were measured with a PHS-3E instrument (Shanghai INESA Scientific Instrument Co., Ltd., China). The Co concentration was analyzed by an atomic absorption spectrophotometer (AAS-300, Perkin-Elmer, USA). All solution samples were measured in transmittance mode from 190 to 900 nm at 1 nm intervals using a quartz cell by an A360 scanning UV/VIS spectrophotometer (AOE Instruments Co., Ltd., Shanghai, China). The morphology changes of the surface of resins were observed using a field-emission scanning electron microscope (FE-SEM; MAIA3 LM; Tescan, USA) with energy dispersive X-ray detector (EDX). Fourier transformed infrared (FTIR) spectra were recorded on a VERTEX 70 Bruker FTIR spectrometer, Germany.

2.4. Computational method

Density functional theory [27] (DFT) calculations were used to investigate the reaction mechanism of cationic resins. The hybrid Becke-3-Lee Yang Parr (B3LYP) density functional method [28] with the 6-31G (d) basis was employed for the geometry optimization and frequency analyses for cationic resins, sulfonated styrene-divinylbenzene monomer, intermediates and products. To eliminate the systematic errors and to obtain a considerably better agreement with the experimental vibrational frequencies, a scaling factor of 0.9613 was applied to the theoretically calculated frequencies [29, 30]. All calculations were carried out using Gaussian 16 package [31].

3. Results and discussion

3.1. Experimental observation

When the reactor was heated under the initial temperature of 75 °C, the Fenton reaction of cationic resins was initiated by the addition of H_2O_2 into the mixture of resins and ferrous solution. The original pH (not adjusted) was about 0.01. During the 180 min of reaction, the evolution of the shape of cationic resins and the color of resin solution can be seen in Fig. 2. At early stage of reaction, the color of resins gradually became black, while the resins started to dissolve. After about 30 min, cationic resins started to completely dissolve. An hour later, all the resin beads turned into yellow liquid. During this period of time, there was a small amount of gas released, and no problem with foaming occurred. The color of resin solution became lighter, and the reaction ended with the formation of a yellow solution in 180 min.

Fenton process used for the decomposition of IERs is primarily based on the efficient generation of hydroxyl radicals (•OH) utilizing ferrous ions as the catalyst to decompose H_2O_2 (reaction 2) [32]. The formed Fe^{3+} can be reduced to Fe^{2+} by H_2O_2 and HOO• according to the reactions (3) and (4), which allows the recycling of Fe^{2+} [9]. Resin beads are first dissolved by the attack of •OH (such as reaction 5), and then the oxidative degradation and mineralization proceeds mainly in aqueous medium [24]. The degradation of the styrene unit and the cross-linking agent can be represented as the reactions (6) and (7), respectively [21].

$$Fe^{2+} + H_2O_2 \rightarrow Fe^{3+} + \bullet OH + OH^- \quad (2)$$

$$Fe^{3+} + H_2O_2 \rightarrow Fe^{2+} + HOO\bullet + H^+ \quad (3)$$

$$Fe^{3+} + HOO\bullet \rightarrow Fe^{2+} + O_2 + H^+ \quad (4)$$

$$C_8H_8SO_3 + 20H_2O_2 \rightarrow 8CO_2 + 23H_2O + H_2SO_4 \quad (5)$$

$$C_8H_8 + 20H_2O_2 \rightarrow 8CO_2 + 24H_2O \quad (6)$$

$$C_{10}H_{10} + 25H_2O_2 \rightarrow 10CO_2 + 30H_2O \quad (7)$$

3.2. Effect of operational parameters on the Fenton oxidation of cationic resins

3.2.1. Effect of initial temperature

The COD value of resin solution changes during the reaction time at various initial temperatures (i.e., 60, 75 and 90 °C) as shown in Fig. 3a. When the initial temperature of reaction was 75 °C, the curve can be divided into two parts: an increase of the COD value followed by a decline stage, which is similar to earlier studies [17, 20]. Peak COD value was reached at about 30 min, indicating that resin beads became almost completely dissolved. Combined with the resin dissolution phenomenon observed in Fig. 2, the increase of the COD value within 30 min could be mainly ascribed to the dissolution of resin beads, whereas the followed decrease of the COD value is due to the degradation of resin solution.

As seen in Fig. 3a, when initial temperature increased from 60 to 75 °C, the complete dissolution time was shortened from 150 to 30 min, while the final COD value of resin solution (after 180 min) was decreased from 7498 to 6057 mg/L. As the initial temperature was further increased to 90 °C, the highest COD value was detected in just 5 min, and COD value was reduced to 2590 mg/L at 180 min,

indicating that higher initial temperature enhances both the dissolution and degradation of cationic resins. An important observation here revealed that even at initial temperature of 60 °C, the complete dissolution of resin beads was obtained. In comparison with other methods, Fenton process for spent resin decomposition can be operated at mild conditions (relatively low temperature and normal pressure), which is a significant advantage for application.

The change of solution temperature during resin decomposition by Fenton process is shown in Fig. 3b. When Fenton reagent was added into the reactor, solution temperature rose, and after the complete addition of Fenton reagent in about 60 min, solution temperature dropped to the initial value, suggesting that the decomposition of resins by Fenton process is exothermic.

3.2.2. Effect of H_2O_2 dosage

The obtained results for resin decomposition as a function of H_2O_2 dosage at various reaction times with 0.3 M Fe^{2+}at pH ≈0.01 and initial temperature of 75 °C are displayed in Fig. 4a. As H_2O_2 dosage increased from 100 to 150 mL, COD value of resin solution increased from 4158 to 6997 mg/L within 10 min, because more radicals formed in the system enhanced the dissolution of cationic resins [11]. After 180 min of reaction, with the increase of H_2O_2 dosage, COD value decreased greatly from 6057 to 1768 mg/L, showing the obviously enhanced degradation of resins, which could be ascribed to the increasing amount of reactive oxidants such as •OH and the dilution by H_2O_2 solution. When H_2O_2 dosage was further increased to 200

mL, the complete dissolution time was shortened from 30 to 15 min, and the final COD value of resin solution was reduced to 498 mg/L.

The degree of cross-linking (DVB) is defined as the mass ratio between cross-linking agent (divinylbenzene, in this study) and cationic resin [33], which is 8% as seen in Table 1. As expressed by reaction (7), the degradation of one mole divinylbenzene consumes 25 moles of H_2O_2 in stoichiometry. Assuming that the mass percentage of poly styrene sulfonic acid (the rest part of cationic resin) is about 92%, the degradation of one mole styrene sulfonic acid consumes 20 moles of H_2O_2 in stoichiometry, as seen in reaction (5). Thus, the theoretical consumption of 30% H_2O_2 (with the density of 1.11 g/cm^3) for 13.55 g dry resin could be calculated as 160 mL. Considering the scavenging effect of hydroxyl radicals by excess H_2O_2 and the decomposition of H_2O_2, adding more H_2O_2 could not effectively improve the dissolution and degradation of resins, but increases the cost of the treatment [21, 34, 35]. Hence, the H_2O_2 dosage of 200 mL was adopted for the decomposition of cationic resins.

3.2.3. Effect of catalyst type and concentration

Oxidation processes using 0.3 M Fe^{2+} and 0.3 M Cu^{2+} as the catalyst for resin decomposition were investigated and compared. From Fig. 4b, we can see that Fe^{2+}/H_2O_2 system is significantly more effective than Cu^{2+}/H_2O_2 system. After 180-min oxidation of resins using Cu^{2+}/H_2O_2, there were still some solid residues left in the final solutions. For cationic resins, higher valence states of metal ions enhance the

absorption and exchange of metal ions with the exchange sites on the resin, increasing the catalytic oxidation of resins [21]. The valence states of Fe^{3+}/Fe^{2+} redox couple are higher than that of Cu^{2+}/Cu^{+} couple, resulting in the higher catalytic ability of Fe^{2+} to the H_2O_2 activation for resin decomposition. Jian et al. [21] also found that cation-exchange resin could be oxidized more efficiently by Fe^{2+} acted as the catalyst than that by other catalysts, such as Cu^{2+}, Ni^{2+}, Mn^{2+}, Ni^{2+}/Cu^{2+} and Mn^{2+}/Cu^{2+}.

The effect of Fe^{2+} concentration on resin decomposition was studied with 200 mL 30% H_2O_2 at pH ≈0.01and initial temperature of 75 °C (Fig. 4c). When the Fe^{2+} concentration increased from 0.1 M to 0.3 M, the time for COD peak value occurred was shortened from 30 min to 15 min, and the final COD value was decreased from 1565 to 498 mg/L, indicating that the increase of Fe^{2+} concentration enhanced both the dissolution and degradation of resins. The enhancing effect could be attributed to the increasing amount of Fe^{2+} absorbed onto the exchange sites of resins producing more reactive oxidants such as •OH [34]. Nevertheless, when the Fe^{2+} concentration was further increased to 0.5 M, the time for COD peak value occurred was prolonged to 20 min, and the final COD value was increased to 1461 mg/L, suggesting that the dissolution and degradation of resins was not further enhanced but a little decreased. Taking into account the total ion exchange capacity of the IER used in this work (4.90 mmol/g), the concentration of Fe^{2+} needed for the saturation of 13.554 g dry resin is calculated as 33 mmol. Under our experimental conditions, 100 mL of 0.1 M, 0.3 M and 0.5 M Fe^{2+} solution amounts to 10, 30 and 50 mmol Fe^{2+}, respectively. Hence,

under conditions where Fe^{2+} concentration is ≤ 0.33 M, Fe^{2+} is practically quantitatively bound to the IER, and the Fenton reaction should take place almost completely at the surface of IER [24]. When the Fe^{2+} concentration was increased above the IER capacity (e.g., 0.5 M), a number of competitive reactions (Eqs. 8 and 9) occurred, negatively affecting the oxidation process [9, 32]. Thus, in our experiment, the optimum Fe^{2+} concentration was 0.3 M.

$Fe^{2+} + \bullet OH \rightarrow Fe^{3+} + OH^-$	(8)
$Fe^{2+} + HOO\bullet \rightarrow Fe^{3+} + HO_2^-$	(9)

3.2.4. Effect of initial pH

The influence of initial pH value on resin dissolution and degradation was investigated at three different pH values of 0.01, 0.76 and 1.01, as shown in Fig. 4d. With the increase of pH, the dissolution and degradation of cationic resins were decreased, which can be mainly ascribed to the reduced formation rate and the lower oxidation potential of •OH [36, 37]. Similar results have been reported by our previous study [9].

3.3. Two-stage first-order kinetics

As Fenton process is very complicated and it produces various reaction intermediates through numerous pathways, it is nearly impossible to simulate each individual reaction. Therefore, a model was used to develop an intrinsic rate equation for COD [14, 18, 19, 34]. The oxidative decomposition rate of Fenton process by using power-law expression was defined by

$$r = -d[COD]/dt = k_0[H_2O_2]^m[COD]^n[Fe^{2+}]^p \quad (10)$$

where k_0 is the rate constant; t is time; $[H_2O_2]$, [COD] and $[Fe^{2+}]$ are values of H_2O_2 dosage, COD and Fe^{2+} concentration, respectively; m, n, p is the order of the reaction. For a given concentration of H_2O_2 and Fe^{2+}, the term of $k_0[H_2O_2]^m[Fe^{2+}]^p$ becomes constant, and the rate expression can be written as

$$r = -d[COD]/dt = k[COD]^n \quad (11)$$

For pseudo-first-order reaction (n = 1), the first-order rate expression is given by

$$\ln[COD]_t = kt + \ln[COD]_0 \quad (12)$$

where $\ln[COD]_0$ is constant.

The kinetics of Fenton oxidation of spent resins was studied, and the effect of initial temperature, H_2O_2 dosage, Fe^{2+} concentration and initial pH was investigated as seen in Fig. 5 and Table 2. It was concluded that the order with respect to COD is 1, since a plot of $\ln[COD]_t$ versus time gives a straight line. The two-stage first-order kinetics composed of the dissolution period of resin beads (first-stage) and the degradation stage of resin solution (second-stage) was observed from Fig. 5a. When the initial temperature increased from 60 to 75°C, the complete dissolution period was shortened, and rate constant of dissolution (k_1) was increased from 0.0064 to 0.0351 min^{-1} (Table 2). As the temperature further increased from 75 to 90 °C, rate constant of degradation (k_2) was increased from 0.0027 to 0.0218 min^{-1}. As shown in Fig. 5b, from 100 to 200 mL H_2O_2 dosage, k_2 was increased from 0.0027 to 0.0507 min^{-1}. Fig. 5c illustrates the effect of Fe^{2+} concentration on the second stage of resin degradation.

When Fe^{2+} concentration increased from 0.1 to 0.5 M, k_2 was first increased from 0.0165 to 0.0507 min^{-1}, and then decreased to 0.0152 min^{-1}. With the increased addition of NaOH, pH value was increased, leading to the inhibition of resin degradation with a decreased k_2 value (Fig. 5d). The trend described in Fig. 5 and the data shown in Table 2 corroborated the effect of operational parameters on the Fenton oxidation of cationic resins discussed in the above section.

3.4. Weight reduction of cationic resins

Fig. 6 shows the effect of initial temperature, H_2O_2 dosage, Fe^{2+} concentration and initial pH on the percentage of weight reduction of cationic resins. As the initial temperature increased from 60 to 90 °C, the weight of residues was reduced from 12.85 to 7.00 g with an increased weight reduction from 5% to 48%. Similarly, lower weight of residues and higher percentage of weight reduction were obtained with higher H_2O_2 dosage. When Fe^{2+} concentration was 0.3 M, the weight of residues was the lowest (3.66 g) with the highest weight reduction rate of 73%. With increasing initial pH value, the weight of residues was increased with decreasing weight reduction rate. These results were consistent with the effect of operational parameters on COD value of cationic resin solution and reaction kinetics during Fenton oxidation observed in the above sections.

The optimum condition derived from the above results was: reaction temperature 90 °C, 200 mL 30% H_2O_2, 0.3 M Fe^{2+} and pH 0.01. At this condition with the initial temperature of 75 °C, the final COD value of resin solution was 498 mg/L with the

degradation rate constant of 0.0507 min^{-1}, and the weight reduction rate reached up to 73%.

3.5. Experimental results on Co-substituted mock samples

During the destruction of spent cationic resins from nuclear power plants, it is also very important to prevent the emission of radionuclides. Thus, the Fenton oxidation of Co-substituted mock samples was studied at 75 °C with 150 mL H_2O_2 and 0.3 M Fe^{2+}, as shown in Fig. 7. Compared with the oxidation of raw resins under similar reaction conditions, it can be found that the decomposition of Co-substituted mock samples was faster than that of raw resins, suggesting that the swelling of the resins caused by the immersion in $CoCl_2 \cdot 5H_2O$ solution enhanced the oxidative destruction of resins [9]. The weight reduction rate of Co-substituted mock samples was 62%, which was also relatively higher than that of raw resins (54%).

After saturated by 0.5 M $CoCl_2 \cdot 6H_2O$ solution, about 5.61 g Co^{2+} were exchanged on the resin surface. Within 180 min Fenton oxidation, about 5.56 g (99%) Co^{2+} was detected in resin decomposition solution, whereas about 0.000122 g (0.0022%) Co^{2+} was analyzed in 2.3 mL condensate of released gases, indicating that the radionuclides loaded in the resins remained in the decomposition solution. Thus, the availability and safety of the resin decomposition by Fenton process are fully verified.

3.6. Decomposition mechanism

The scanning electron microscopy (SEM) analyses were performed to investigate the morphological change of resins during disintegration process. Fig. 8 exhibits the

SEM images of dried fresh cationic resin beads and resin residue after 10 min, 30 min, 90 min and 180 min reaction. The surface of spherical beads became no longer smooth and were cracked within 10 min (Figs. 8b and 8c), which was resulted from the attack of hydroxyl radicals. Then the resin beads started disintegration and fragmentation until they were completely dissolved after 30 min (Fig. 8d), which corroborated the experimental observation and two-stage first-order kinetics discussed in the above section. The matrix crack and the resin disintegration was probably expected to the desulfonation of the aromatic rings, oxidative fragmentation of the polymer backbone and mineralization of decomposition solution by the attack of •OH and high pressure of CO_2 formed through the reactions (5)−(7) [10, 18].

For the Co-substituted mock samples, the SEM observation of resin disintegration process is shown in Fig. 9. The diameter of resins was 503 μm after soaking with Co^{2+} solution (Fig. 9a), larger than that of fresh resins (363 μm, Fig. 8a), indicating the swelling of the resins after immersion, which further corroborated the faster decomposition of Co-substituted mock samples observed in Fig. 7. The EDX spectra (Fig. 9b) confirmed that Co^{2+} ions were exchanged on the resin surface. After 180 min reaction, according to the surface morphology of dried samples as seen in Fig. 9c., the resin beads were cracked. EDX analysis as seen in Fig. 9d displayed the existence of Co and the Fe catalyst in the resin residue.

Ultraviolet-visible spectroscopy (Figs. 10 and 12) was used to verify the color of organics as well as to speculate the molecular structure, because organic compounds

absorbing light in the UV or visible regions of the electromagnetic spectrum directly affects the molecular structure and the perceived color of the chemicals involved [38–40]. From Fig. 10, it can be seen that the degradation solution of resins was a dark color in twenty-time diluted solution after 5 min and 10 min reaction, and turned dark brown after 20 min with the corresponding absorption peaks blue-shift to shorter wavelengths. The color of resin solution was gradually lightened, showing an orange-yellow at 30 min, with the absorption band below 450 nm. Finally, a yellow solution was observed, which is consistent with the experimental observation in Section 3.1.

Because the cationic exchange resin used in this study is prepared by sulfonation of polystyrene cross-linked with divinyl benzene, sulfonated styrene-divinylbenzene monomer is modeled with the calculated bond length and energy to study the resin structure and decomposition mechanism as seen in Fig. 11. The distances of C4–C5, C5–C6 and C8–S9 bonds are 1.5415, 1.5460 and 1.7822 Å, respectively, relatively longer than other bonds, exhibiting smaller bond energies, which indicate that these bonds are weaker bonds and easier to be broken [41, 42].

After the cleavage of C4–C5, C5–C6 and C8–S9 bonds, the degradation intermediates of resin, such as ethylbenzenesulfonic acid, sulfobenzoic acid, ethylphenol, 4-ethylbenzoic acid, 1-(2-hydroxyphenyl) ethanone, 1-(3-hydroxyphenyl) ethanone, 1-(4-hydroxyphenyl) ethanone, hydroxybenzoic acid, phthalic acid, benzenediol, benzoquinone and small molecule acids, were speculated [43, 44]. The corresponding UV spectroscopic data of sulfonated styrene-

divinylbenzene monomer and these intermediate compounds were calculated by Gaussian 16 package for the wavelengths between 150 nm and 400 nm (Figs. 12b–e). The ultraviolet spectrum (between 190 nm and 400 nm) of resin solution during Fenton oxidation experiment was observed as shown in Fig. 12a. After 5 min of reaction, the absorption bands of the resin solution were observed in the 220–260 nm region (Fig. 12a), related mainly to sulfonated styrene-divinylbenzene monomers (Fig. 12b), and 200–240 nm which are principal absorptions of benzene ring compounds such as 4-ethylbenzoic acid, phthalic acid (Fig. 12c), sulfobenzoic acid (Fig. 12d) and other phenolic compounds. After 10 min of reaction, more absorption bands were observed at longer wavelengths (260−290 nm) in the UV spectrum (Fig. 12a), which indicated that the fracture of carbon frame, desulfonation and detachment of benzene ring from carbon frame might happen, and more intermediates were produced during the Fenton oxidation. These absorptions might be related to hydroxyphenyl ethanone, hydroxybenzoic acid, benzenediol and benzoquinone (Fig. 12c). The absorption bands of the resin solution at 20 min and 30 min were observed from 195 to 230 nm, and absorptions around 230–260 nm diminished (Fig. 12a), suggesting that resin beads (mainly sulfonated dstyrene-divinylbenzene monomers as seen in Fig. 12b) were decomposed into organic intermediates as the aromatic-ring opening occurring, such as hydroxyphenyl ethanone, hydroxybenzoic acid, phthalic acid (Fig. 12c), 4-ethylbenzenesulfonic acid, 2-sulfobenzoic acid, 3-sulfobenzoic acid (Fig. 12d), maleic acid and fumarid acid (Fig. 12e). It should be noted that after

30min, similar UV spectra were obtained, which showed an absorption peak at the shorter wavelength (195 nm), further verified the two-stage decomposition of resins. The UV spectra indicated that the structure might be 2-ethylbenzenesulfonic acid, 3-ethylbenzenesulfonic acid, 2-sulfobenzoic acid, ethylphenol, benzenediol, oxalic acid, etc., which eventually remained in solution.

The FTIR spectra have also been used in the elucidation of structural performance of the cationic resin and its oxidized products [1, 10, 45]. The FTIR spectra of resin monomers and oxidized products were studied using DFT methods, which were compared with experimental results to analyze the molecular structure precisely [46, 47]. The comparison of experimental FTIR spectrum of the fresh resin and calculated results of sulfonated styrene-divinylbenzene monomer are shown in Fig. 13, and the structures are listed in Table 3. The characteristic bands at about 3500 and 1640 cm^{-1} in the experimental FTIR spectrum are probably attributed to the interference of H_2O. The bands corresponding to C-H stretching vibration are identified at 2926 and 2992 cm^{-1}. The observed region of 1674−1349 cm^{-1} corresponds to the C-H in-plane vibration on the carbon skeleton and benzene ring of the resin, the C=C stretching on the benzene ring and the associated complex vibration. The bands appearing at 1147 and 1120 cm^{-1} are assigned to the sulfonic groups (C-S and S=O wagging vibration). Several bands in the region of 1030 to 561 cm^{-1} are observed, corresponding to the stretching and deformation of benzene ring. The detailed dynamic characteristics of these vibration patterns can be seen in the supplementary material (slides 1−3).

The changes of experimental FTIR spectra during the Fenton oxidation of resins at 75 °C with 200 mL H_2O_2 and 0.3 M Fe^{2+} are shown in Fig. 14. Based on the calculated FTIR spectra of the speculated intermediates of resin (Figs. S1−S4, supplementary material), the experimental FTIR bands and tentative assignments are displayed in Table 4. After 10 min of reaction, there is little change in the FTIR spectrum compared with the experimental FTIR spectrum of the fresh resin, which is consistent with the SEM and UV analyses. The lower intensity of the characteristic bands at 1120, 1031, 1002, 833, 774, 669 and 560 cm^{-1}, associated with $–SO_3H$, C-H vibration on the benezene ring, O-H in-plane wagging of hydroxyl and carboxyl groups, phenolic hydroxyl groups, benzene ring deformation and C-H wagging of aliphatic groups, may be related to the oxidation of carbon skeleton and sulfonic acid groups of resins by •OH. In the 30-min sample, some bands associated to C-H stretching vibration of aliphatic groups disappears, and an important feature is observed at 3403 cm^{-1} corresponding to O-H stretching of hydroxyl groups. The bands at 1665, 1291 and 1173 cm^{-1} exhibit a higher intensity, which is possibly due to the formation of carboxylic acids. Meanwhile, relevant increase of bands appeared at 1173−850 cm^{-1}, associated to C-H vibration of benzene ring, C-O or C-C stretching, O-H wagging, indicating that many aromatic substances based on benzene ring substitution with •OH are produced. The corresponding substances containing sulfonic groups are significantly reduced, which is speculated that most of the sulfonic groups on the resins are directly broken or substituted with •OH forming phenolic

hydroxyl groups. The carbon skeleton of resins is cracked and oxidized by •OH, generating Carbonyl-containing carboxylic acids, ketones, aldehydes, etc. These results further vierify the dissolution stage of resin beads (first-stage) mostly ascribed to the desulfonation of resin molecules and the oxidative fragmentation of the carbon skeleton. After a 90 min reaction, the characteristic bands associated with the carbonyl, hydroxyl groups and their complex vibration exihibit a higher intensity, indicating the formation of carboxylic acid substances. The sulfonic acid species disappeared, and the corresponding substances with fatty groups also decreased, speculating that the sulfonic groups and the carbon skeleton almost disappeared, and some benzene rings are broken and oxidized to carboxylic acids. From the FTIR spectrum of 180-min sample, many bands disappear, only left the main features appear at 1646 cm^{-1} (H_2O, benzene ring vibration and C=O stretching), 1465 and 1417 cm^{-1} (C=C stretching and C-H vibration on the benzene ring, C-H wagging), 1004 cm^{-1} (SO_4^{2-}, H wagging on the C=C bond), 656 and 575 cm^{-1} (SO_4^{2-}, O-H out-of-plane deformation of carboxylic acids). There are still some benzene compounds such as phenol, benzenediol, benzoic acid and terephthalic acid remaining in solution. At the same time, some of the benzene rings are oxidized and opened to form saturated and unsaturated acids, with a high concentration of sulfate leaving in solution.

Based on the above analysis, the cation resin degradation mechanism was inferred. The oxidation and mineralization of organic pollutants by Fenton process are

principally induced by •OH via hydrogen abstraction, electrophilic addition to π-systems and electron transfer [24, 48, 49]. For cationic resins used in this work, Fe^{2+} was initially exchanged with H^+ on the IER, and Fenton reactions first occurred on the resin beads. Hydroxyl radicals produced by Fenton reactions on the IER first initiate the oxidative fragmentation of the polymer backbone (the breakdown of C5–C6 bond, Eq. 12) as well as the desulfonation of the sulfonated aromatic rings (Eqs. 5 and 13) [24]. Hydrogen abstraction would mainly concern the tertiary C-centers of the polystyrene backbone for oxidative fragmentation (reaction 12) [24]. As shown in reaction (13), electrophilic addition of •OH to π-systems would happen on the aromatic moieties of the polymer substrate for desulfonation [24]. After the first stage of dissolution of resin beads, complex substituents on the benzene ring were oxidized and replaced by simpler carboxyl and hydroxyl groups, which were further oxidized by •OH to form quinones, especially p-benzoquinone, and then oxidized to form ring-opening unsaturated acids and saturated acids. These carboxylic acids might be finally oxidized to CO_2 and H_2O (Eqs. 5−7).

$$C_8H_8SO_3 + 20H_2O_2 \rightarrow 8CO_2 + 23H_2O + H_2SO_4 \quad (5)$$

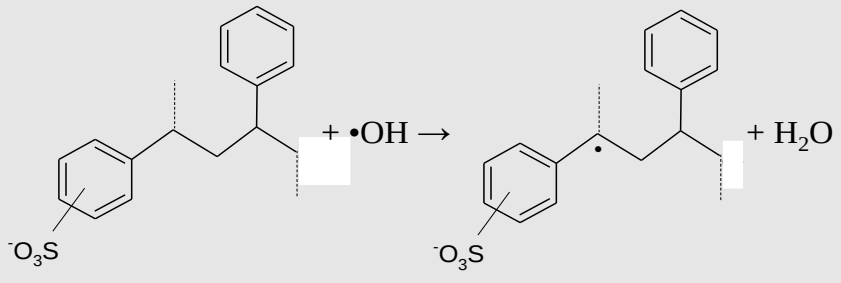

(12)

4. Conclusions

Fenton oxidation has been proven to be a potential and promising method for the

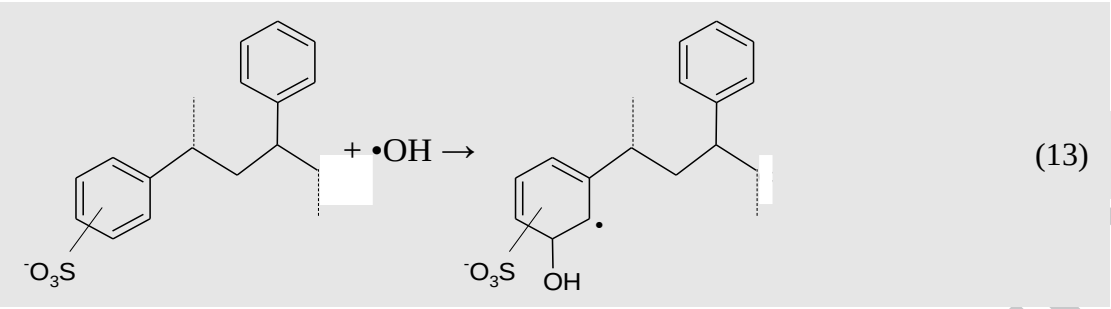

(13)

dissolution and degradation of cationic resins. The operational parameters, such as initial temperature and pH, H_2O_2 dosage, catalyst type and concentration, were investigated and optimized. Complete dissolution of cationic resins and minimum COD value were obtained with H_2O_2 200 mL, Fe^{2+} 0.3 M at initial temperature 75 °C and pH 0.01, corresponding to a weight reduction of 73%. The two-stage first-order kinetics was observed during the oxidation of cationic resins, which was composed of a dissolution stage of resin beads mostly ascribed to the desulfonation of resin molecules and the oxidative fragmentation of the polymer backbone by •OH, and a followed degradation stage of resin solution mainly ascribed to the oxidation of intermediates by •OH in aqueous medium. It is concluded that wet oxidation using the Fenton reagent is an effective pretreatment method to reduce the amount of the spent resins.

Acknowledgements:

This work was supported by the National Natural Science Foundation of China (Grant No. 51708238), and the National Natural Science Foundation special fund for Thousands Plan Youth Talent (No. 0222120003; 0214120048). The authors would also like to thank the financial support provided by State Administration of Science, Technology and Industry for National Defense, PRC (Grant No. 2017-1237).

References

[1] S. Ghosh, K. Dhole, M.K. Tripathy, R. Kumar, R.S. Sharma, FTIR spectroscopy in the characterization of the mixture of nuclear grade cation and anion exchange resins, J. Radioanal. Nucl. Chem. 304 (2015) 917–923.

[2] P.U. Singare, Ion-isotopic exchange reaction kinetics using organic base anion exchange resins Indion-102 and Indion GS-400, Colloid J. 76 (2014) 637–643.

[3] J.L. Wang, Z. Wan, Treatment and disposal of spent radioactive ion-exchange resins produced in the nuclear industry, Prog. Nucl. Energy 78 (2015) 47–55.

[4] J.F. Li, J.L. Wang, Advances in cement solidification technology for waste radioactive ion exchange resins: A review, J. Hazard. Mater. 135 (2006) 443–448.

[5] Q.N. Sun, J.F. Li, J.L. Wang, Solidification of borate radioactive resins using sulfoaluminate cement blending with zeolite, Nucl. Eng. Des. 241 (2011) 5308–5315.

[6] U.K. Chun, K. Choi, K.H. Yang, J.K. Park, M.J. Song, Waste minimization pretreatment via pyrolysis and oxidative pyrolysis of organic ion exchange resin, Waste Manage. 18 (1998) 183–196.

[7] R.S. Juang, T.S. Lee, Oxidative pyrolysis of organic ion exchange resins in the presence of metal oxide catalysts, J. Hazard. Mater. 92 (2002) 301–314.

[8] Y. Kobayashi, H. Matsuzuru, J. Akatsu, N. Moriyama, Acid digestion of radioactive combustible wastes: Use of hydrogen peroxide for acid digestion of ion exchange resins, J. Nucl. Sci. Technol. 17 (1980) 865–868.

[9] Z. Wan, L.J. Xu, J.L. Wang, Disintegration and dissolution of spent radioactive

cationic exchange resins using Fenton-like oxidation process, Nucl. Eng. Des. 291 (2015) 101–108.

[10] Z. Wan, L.J. Xu, J.L. Wang, Treatment of spent radioactive anionic exchange resins using Fenton-like oxidation process, Chem. Eng. J. 284 (2016) 733–740.

[11] S. Chong, G.M. Zhang, N. Zhang, Y.C. Liu, T. Huang, H.Z. Chang, Diclofenac degradation in water by $FeCeO_x$ catalyzed H_2O_2: Influencing factors, mechanism and pathways, J. Hazard. Mater. 334 (2017) 150–159.

[12] Y.C. Liu, G.M. Zhang, S. Chong, N. Zhang, H.Z. Chang, T. Huang, S.Y. Fang, $NiFe(C_2O_4)_x$ as a heterogeneous Fenton catalyst for removal of methyl orange, J. Environ. Manage., 192 (2017) 150–155.

[13] M.A. Dubois, J.F. Dozol, C. Massiani, M. Ambrosio, Reactivities of polystyrenic polymers with supercritical water under nitrogen or air. Identification and formation of degradation compounds, Ind. Eng. Chem. Res. 35 (1996) 2743–2747.

[14] Y. Akai, K. Yamada, T. Sako, Ion-exchange resin decomposition in supercritical water, High Pressure Res. 20 (2001) 515–524.

[15] K. Kim, K. Kim, M. Choi, S.H. Son, J.H. Han, Treatment of ion exchange resins used in nuclear power plants by super- and sub-critical water oxidation - A road to commercial plant from bench-scale facility, Chem. Eng. J. 189 (2012) 213–221.

[16] K. Kim, S.H. Son, K. Kim, J.H. Han, K. Do Han, S.H. Do, Treatment of radioactive ionic exchange resins by super- and sub-critical water oxidation (SCWO), Nucl. Eng. Des. 240 (2010) 3654–3659.

[17] C.T. Yu, C.F. Wang, W.Z. Wang, Decomposition of organic resin by radio-sensitive photocatalyst, J. Photochem. Photobiol. A: Chem. 186 (2007) 369–375.

[18] T.L. Gunale, V.V. Mahajani, P.K. Wattal, C. Srinivas, Studies in liquid phase mineralization of cation exchange resin by a hybrid process of Fenton dissolution followed by wet oxidation, Chem. Eng. J. 148 (2009) 371–377.

[19] T.L. Gunale, V.V. Mahajani, P.K. Wattal, C. Srinivas, Liquid phase mineralization of gel-type anion exchange resin by a hybrid process of Fenton dissolution followed by sonication and wet air oxidation, Asia-Pac. J. Chem. Eng. 4 (2009) 90–98.

[20] P.A. Taylor, Destruction of ion-exchange resin in waste from the HFIR, T1, and T2 tanks using Fenton's reagent, ORNL/TM-2002/197. (2002).

[21] X.C. Jian, T.B. Wu, G.C. Yun, A study of wet catalytic oxidation of radioactive spent ion exchange resin by hydrogen peroxide, Nucl. Saf. 37 (1996) 149–157.

[22] Y.C. Ye, S.N. Yu, Stabilization and volume reduction of radioactive spent ion exchange resins, Nucl. Sci. Tech. 12 (2001) 68–72.

[23] M. Zahorodna, R. Bogoczek, E. Oliveros, A.M. Braun, Application of the Fenton process to the dissolution and mineralization of ion exchange resins, Catal. Today 129 (2007) 200–206.

[24] M. Zahorodna, E. Oliveros, M. Wörner, R. Bogoczek, A.M. Braun, Dissolution and mineralization of ion exchange resins: differentiation between heterogeneous and homogeneous (photo-)Fenton processes, Photochem. Photobiol. Sci. 7 (2008) 1480–1492.

[25] Z. Wan, J.L. Wang, Optimization of spent radioactive resins degradation by Fenton-like oxidation using response surface methodology, Environ. Prog. Sustain. Energy 35 (2016) 1590–1596.

[26] Standard of the People's Republic of China for Environmental Protection, Water quality-Determination of the chemical oxygen demand-Fast digestion-spectrophotometric method, HJ/T 399-2007.

[27] A.D. Becke, J. Chem, Density-functional thermochemistry. III. The role of exact exchange, Phys. 98 (1993) 5648–5652.

[28] C. Lee, W. Yang, R.G. Parr, Development of the Colle-Salvetti correlation-energy formula into a functional of the electron density, Phys. Rev. B 37 (1988) 785–789.

[29] J.B. Foresman, P.A. Pittsburg, in: E. Frisch (Ed.), Exploring chemistry with electronic structure methods: A guide to using Gaussian, (1996).

[30] S. Beegum, Y.S. Mary, H.T. Varghese, C.Y. Panicker, S. Armaković, S.J. Armaković, J. Zitko, M. Dolezal, C. Van Alsenoy, Vibrational spectroscopic analysis of cyanopyrazine-2-carboxamide derivatives and investigation of their reactive properties by DFT calculations and molecular dynamics simulations, J. Mol. Struct. 1131 (2017) 1–15.

[31] M.J. Frisch, G.W. Trucks, H.B. Schlegel, G.E. Scuseria, M.A. Robb, J.R. Cheeseman, G. Scalmani, V. Barone, G.A. Petersson, H. Nakatsuji, X. Li, M. Caricato, A.V. Marenich, J. Bloino, B.G. Janesko, R. Gomperts, B. Mennucci, H.P. Hratchian, J.V. Ortiz, A.F. Izmaylov, J.L. Sonnenberg, Williams, F. Ding, F. Lipparini,

F. Egidi, J. Goings, B. Peng, A. Petrone, T. Henderson, D. Ranasinghe, V.G. Zakrzewski, J. Gao, N. Rega, G. Zheng, W. Liang, M. Hada, M. Ehara, K. Toyota, R. Fukuda, J. Hasegawa, M. Ishida, T. Nakajima, Y. Honda, O. Kitao, H. Nakai, T. Vreven, K. Throssell, J.A. Montgomery, Jr., J.E. Peralta, F. Ogliaro, M.J. Bearpark, J.J. Heyd, E.N. Brothers, K.N. Kudin, V.N. Staroverov, T.A. Keith, R. Kobayashi, J. Normand, K. Raghavachari, A.P. Rendell, J.C. Burant, S.S. Iyengar, J. Tomasi, M. Cossi, J.M. Millam, M. Klene, C. Adamo, R. Cammi, J.W. Ochterski, R.L. Martin, K. Morokuma, O. Farkas, J.B. Foresman, D.J. Fox, Gaussian 16, Gaussian Inc.: Wallingford, CT, (2016).

[32] J.L. Wang, L.J. Xu, Advanced oxidation processes for wastewater treatment: Formation of hydroxyl radical and application, Crit. Rev. Environ. Sci. Technol. 42 (2012) 251–325.

[33] L. Wilson, A. Manes, L. Soler, M.J. Henríquez, Effect of the degree of cross-linking on the properties of different CLEAs of penicillin acylase, Process Biochem. 44 (2009) 322–326.

[34] L.J. Xu, J.L. Wang, A heterogeneous Fenton-like system with nanoparticulate zero-valent iron for oxidation of 4-chloro-3-methyl phenol, J. Hazard. Mater. 186 (2011) 256–264.

[35] J.Q. Shi, T. Long, R.R. Ying, L. Wang, X. Zhu, Y.S. Lin, Chemical oxidation of bis(2-chloroethyl) ether in the Fenton process: Kinetics, pathways and toxicity assessment, Chemosphere 180 (2017) 117–124.

[36] R.M. Liou, S.H. Chen, M.Y. Hung, C.S. Hsu, J.Y. Lai, Fe (III) supported on resin as effective catalyst for the heterogeneous oxidation of phenol in aqueous solution, Chemosphere 59 (2005) 117–125.

[37] M. Vilve, S. Vilhunen, M. Vepsäläinen, T.A. Kurniawan, N. Lehtonen, H. Isomäki, M. Sillanpää, Degradation of 1,2-dichloroethane from wash water of ion-exchange resin using Fenton's oxidation, Environ. Sci. Pollut. Res. 17 (2010) 875–884.

[38] N. Sertova, I. Petkov, J.M. Nunzi, Photochromism of mercury(II) dithizonate in solution, J. Photochem. Photobiol. A: Chem. 134 (2000) 163–168.

[39] Z.Q. Yan, S.Y. Guang, H.Y. Xu, X.Y. Su, X.L. Ji, X.Y. Liu, Supramolecular self-assembly structures and properties of zwitterionic squaraine molecules, RSC Adv. 3 (2013) 8021–8027.

[40] M.J. Martelo-Vidal, M. Vázquez, Advances in ultraviolet and visible light spectroscopy for food authenticity testing, in: G. Downey (Ed.) Advances in Food Authenticity Testing, (2016) 35–70.

[41] M. Kaupp, B. Metz, H. Stoll, Breakdown of bond length-bond strength correlation: A case study, Angew. Chem. Int. Ed. 39 (2000) 4607–4609.

[42] A.A. Zavitsas, The relation between bond lengths and dissociation energies of carbon-carbon bonds, J. Phys. Chem. A 107 (2003) 897–898.

[43] Y. Liu, B.L. Yang, C.H. Yi, Density functional theory investigation for catalytic mechanism of gasoline alkylation desulfurization over NKC-9 ion-exchange resin,

Ind. Eng. Chem. Res. 52 (2013) 6933–6940.

[44] A. Leybros, A. Roubaud, P. Guichardon, O. Boutin, Supercritical water oxidation of ion exchange resins: Degradation mechanisms, Process Saf. Environ. Prot. 88 (2010) 213–222.

[45] Z.Q. Yan, S.Y. Guang, H.Y. Xu, X.Y. Liu, Quinoline-based azo derivative assembly: Optical limiting property and enhancement mechanism, Dyes Pigm. 99 (2013) 720–726.

[46] Y.I. Zhang, H.Y. Wang, D.S. Jiao, Y.H. Hu, Density functional theory study of infrared and ultraviolet spectra of urea L-malic acid, Chin. J. Chem. Phys. 21 (2008) 535–540.

[47] D. Sajan, G.D. Sockalingum, M. Manfait, I. Hubert Joe, V.S. Jayakumar, NIR-FT Raman, FT-IR and surface-enhanced Raman scattering spectra, with theoretical simulations on chloramphenicol, J. Raman Spectrosc. 39 (2008) 1772–1783.

[48] L.J. Xu, J.L. Wang, Magnetic nanoscaled Fe_3O_4/CeO_2 composite as an efficient Fenton-like heterogeneous catalyst for degradation of 4-chlorophenol, Environ. Sci. Technol. 46 (2012) 10145–10153.

[49] L.J. Xu, J.L. Wang, Fenton-like degradation of 2,4-dichlorophenol using Fe_3O_4 magnetic nanoparticles, Appl. Catal. B: Environ. 123 (2012) 117–126.

Figure captions

Figure 1. Schematic diagram of the experimental set-up used for the Fenton oxidation of cationic resins.

Figure 2. Evolution of the shape and color of resin solution during the Fenton process with 0.3 M Fe^{2+} and 100 mL H_2O_2 at pH ≈ 0.01 and initial temperature of 75 °C.

Figure 3. (a) Effect of initial temperature on the dissolution and degradation of cationic resins; (b) the change of solution temperature during resin decomposition by Fenton process. Reactions were conducted with 0.3 M Fe^{2+} and 100 mL H_2O_2 at pH ≈ 0.01.

Figure 4. Effects of (a) H_2O_2 dosage, (b) catalyst type, (c) Fe^{2+} concentration, and (d) initial pH on resin decomposition. Except for the investigated parameter, other parameters fixed on *T*75 °C, H_2O_2 200 mL, Fe^{2+} 0.3 M and pH ≈ 0.01.

Figure 5. Pseudo-first-order plots for resin dissolution and degradation by Fenton process: (a) effect of initial temperature; (b) effect of H_2O_2 dosage; (c) effect of Fe^{2+} concentration; (d) effect of initial pH. Except for the investigated parameter, other parameters fixed on *T*75 °C, H_2O_2 200 mL, Fe^{2+} 0.3 M and pH ≈ 0.01.

Figure 6. The percentage of weight reduction at different operational conditions. Except for the investigated parameter, other parameters fixed on *T*75 °C, H_2O_2 200 mL, Fe^{2+} 0.3 M and pH ≈ 0.01.

Figure 7. Decomposition of raw resins and Co-substituted mock samples at 75 °C with 150 mL H_2O_2 and 0.3 M Fe^{2+}.

Figure 8. SEM images of spent resin during decomposition process at 75 °C with 200 mL H_2O_2 and 0.3 M Fe^{2+}: (a) fresh cationic resin beads, 500×; (b) after 10 min,500×; (c) after 10 min, 10000×; (d) after 30 min,500×; (e) after 90 min, 500×; (f) after 180 min, 300×.

Figure 9. SEM images and EDX spectra of Co-substituted mock samples (a, b) and decomposition residue after 180 min (c, d).

Figure 10. Ultraviolet-visible spectrum of resin solution during decomposition process at 75 °C with 200 mL H_2O_2 and 0.3 M Fe^{2+}.

Figure 11. Optimized geometries of the model of sulfonated styrene-divinylbenzene monomer with calculated bond length and energy. The units of length and energy are angstrom (Å) and kJ/mol, respectively.

Figure 12. Ultraviolet spectrum of resin solution during decomposition process at 75 °C with 200 mL H_2O_2 and 0.3 M Fe^{2+} (a), and calculated UV spectroscopic data of sulfonated styrene-divinylbenzene monomer and intermediate compounds (b–e).

Figure 13. The experimental FTIR spectrum of the fresh resin and calculated FTIR spectrum of sulfonated styrene-divinylbenzene monomer.

Figure 14. The changes of the FTIR spectrum of resin during decomposition process at 75 °C with 200 mL H_2O_2 and 0.3 M Fe^{2+}.

Figure 1

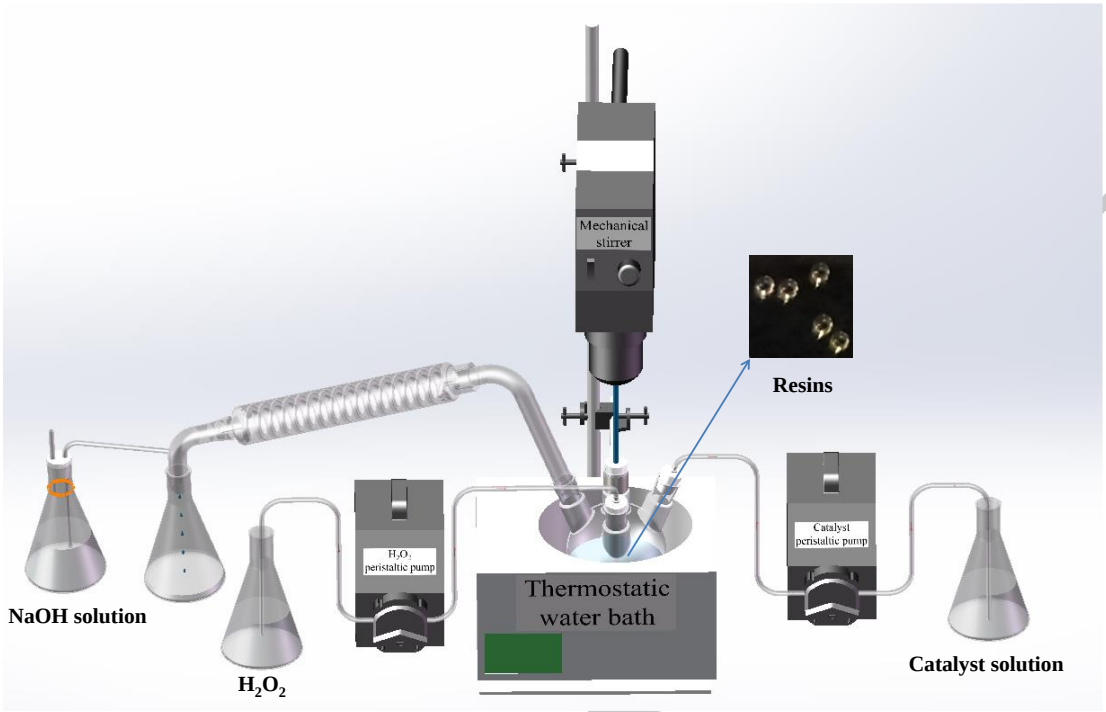

Figure 2

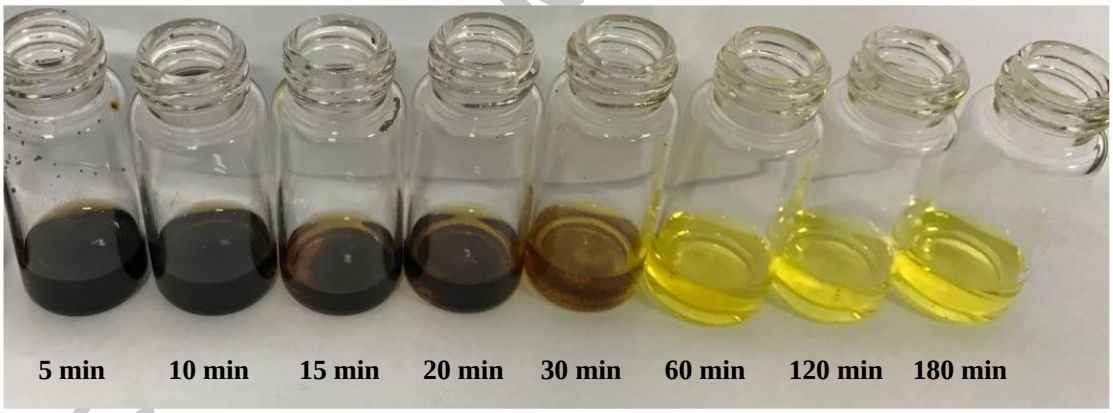

Figure 3

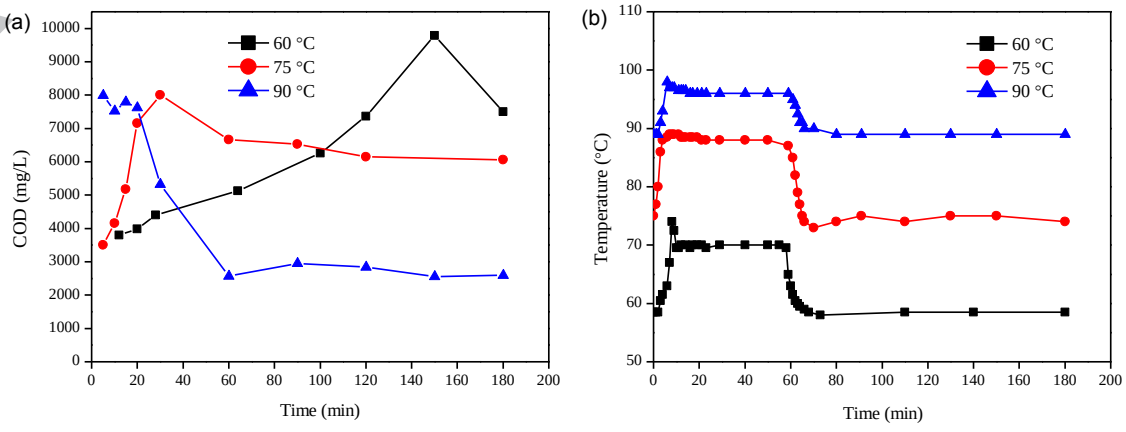

Figure 4

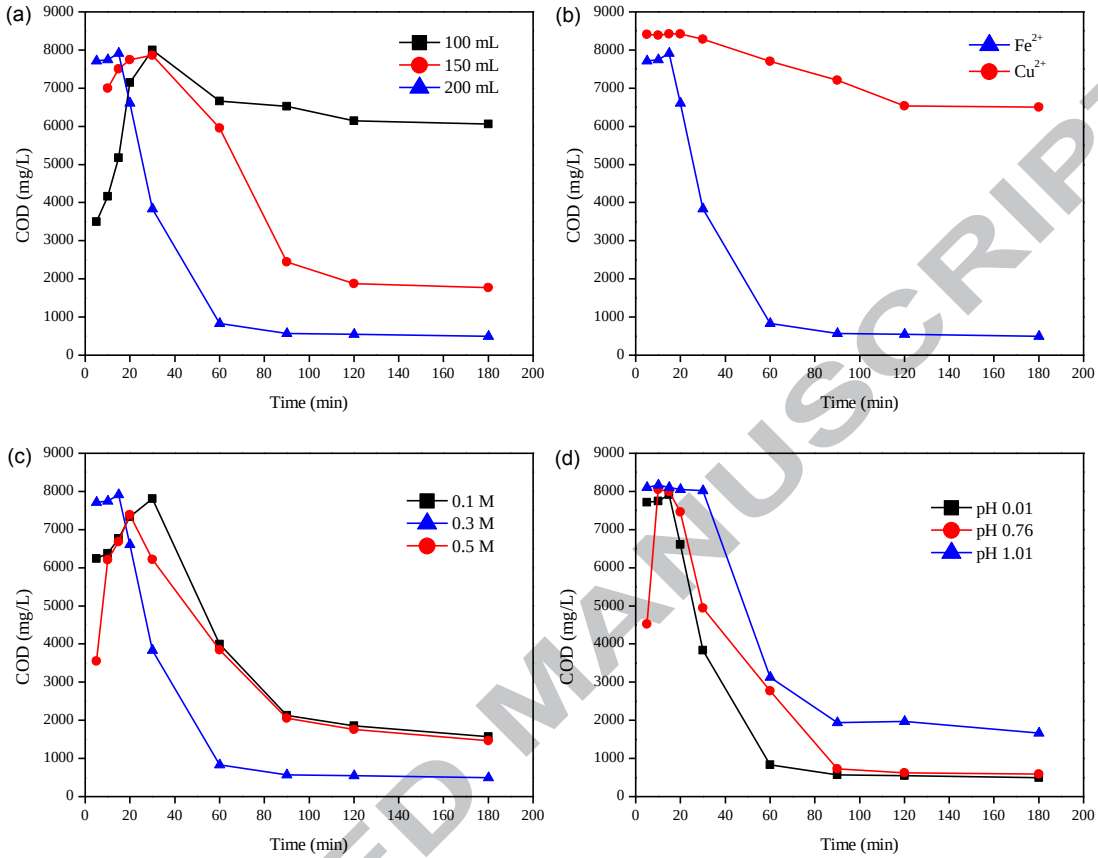

Figure 5

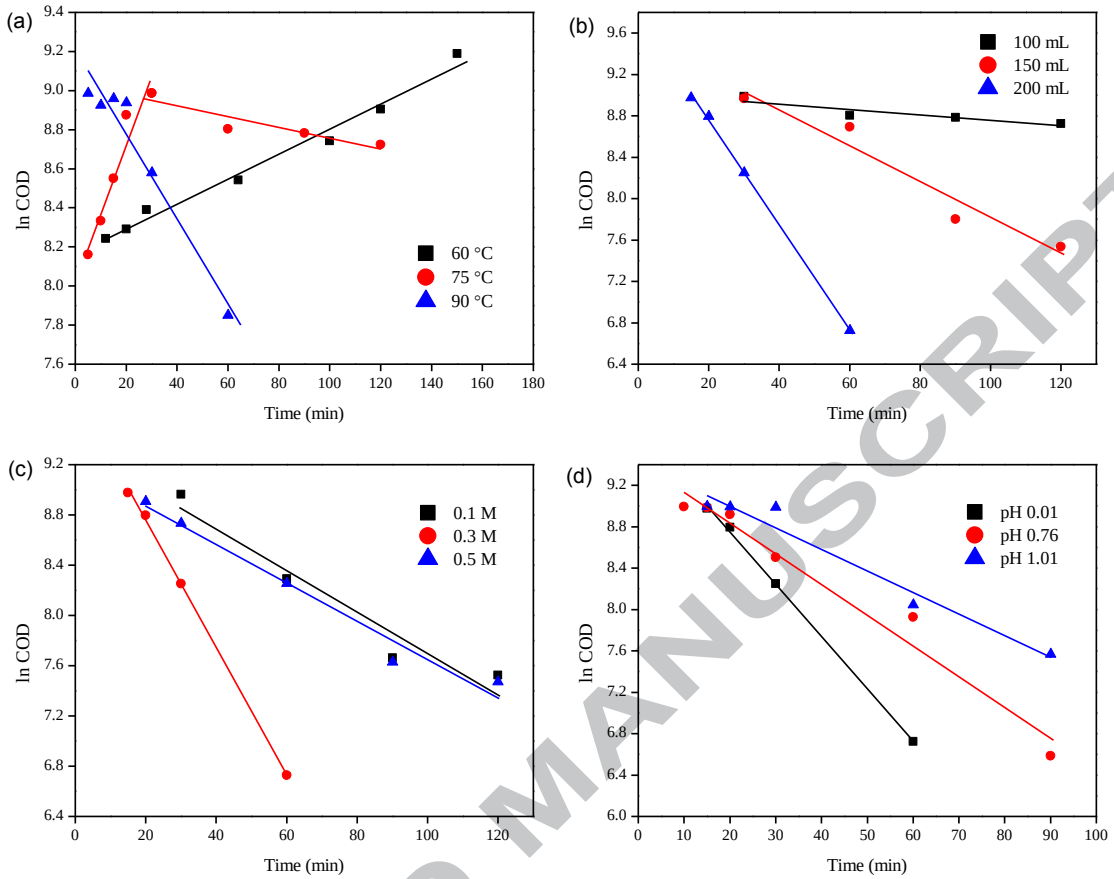

Figure 6

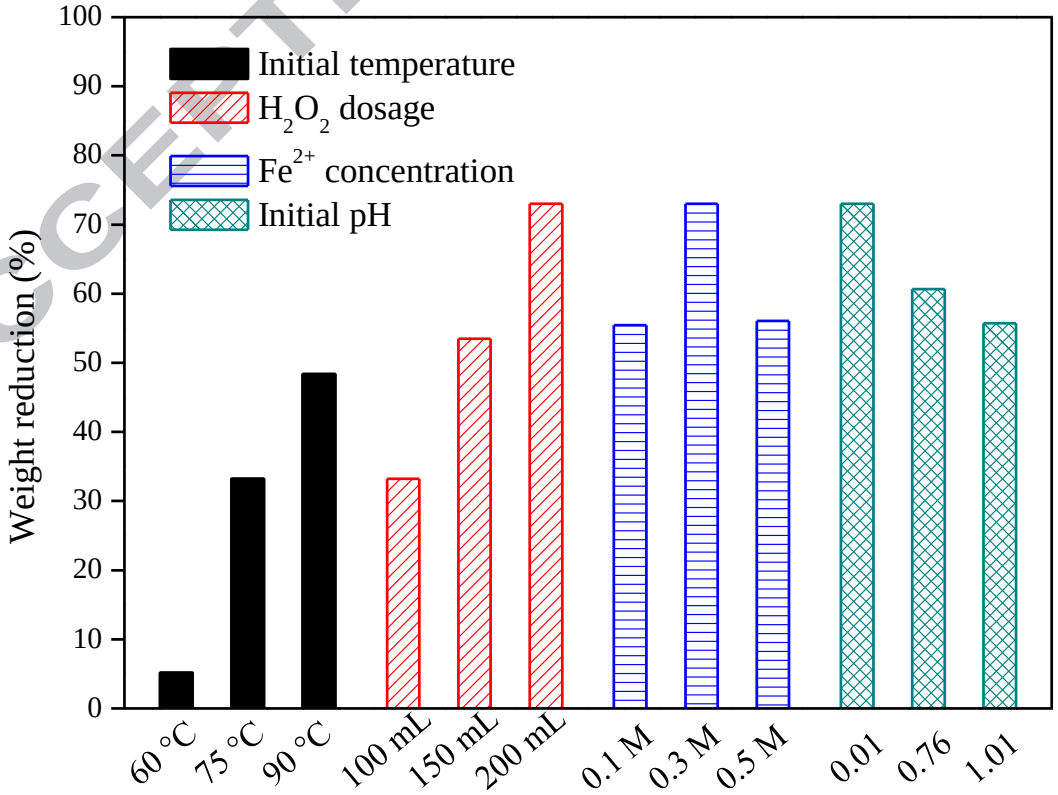

Figure 7

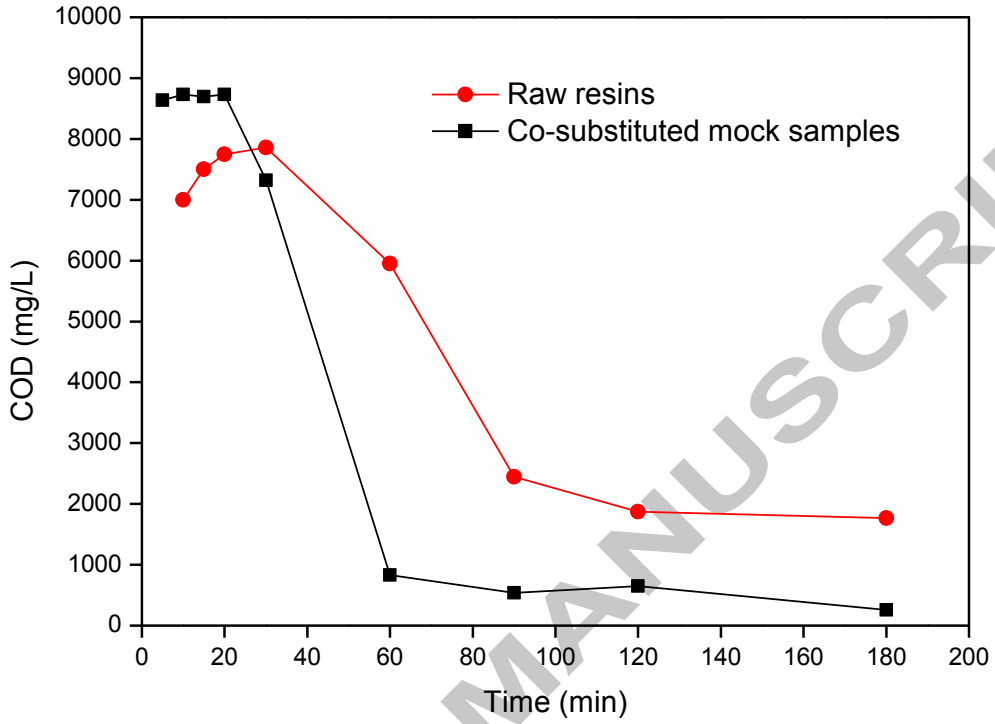

Figure 8

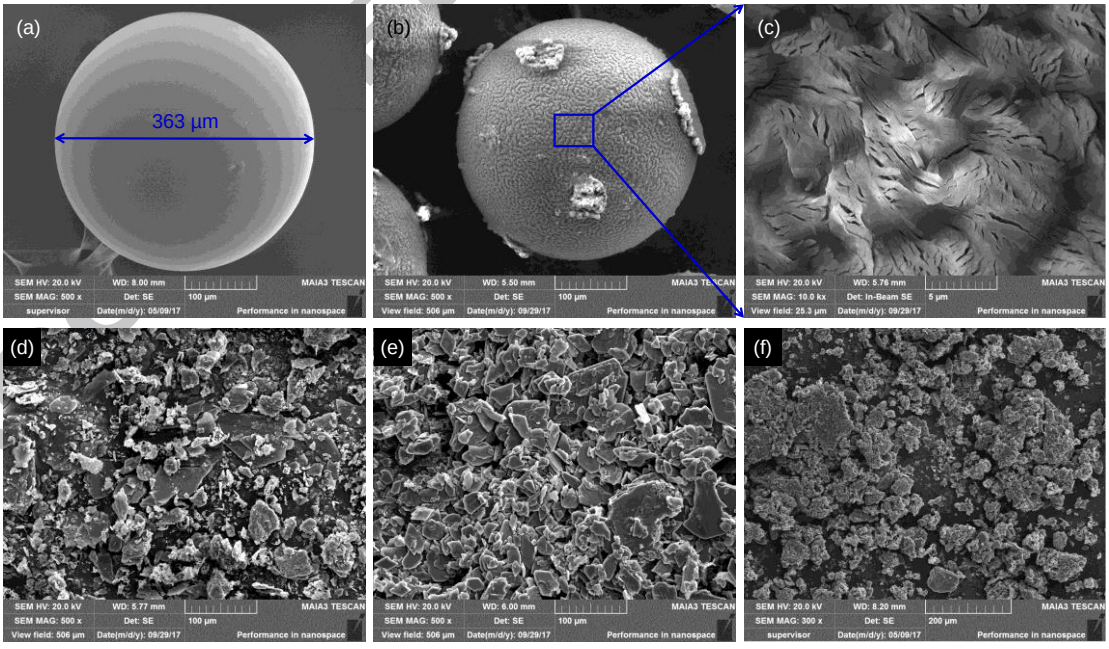

Figure 9

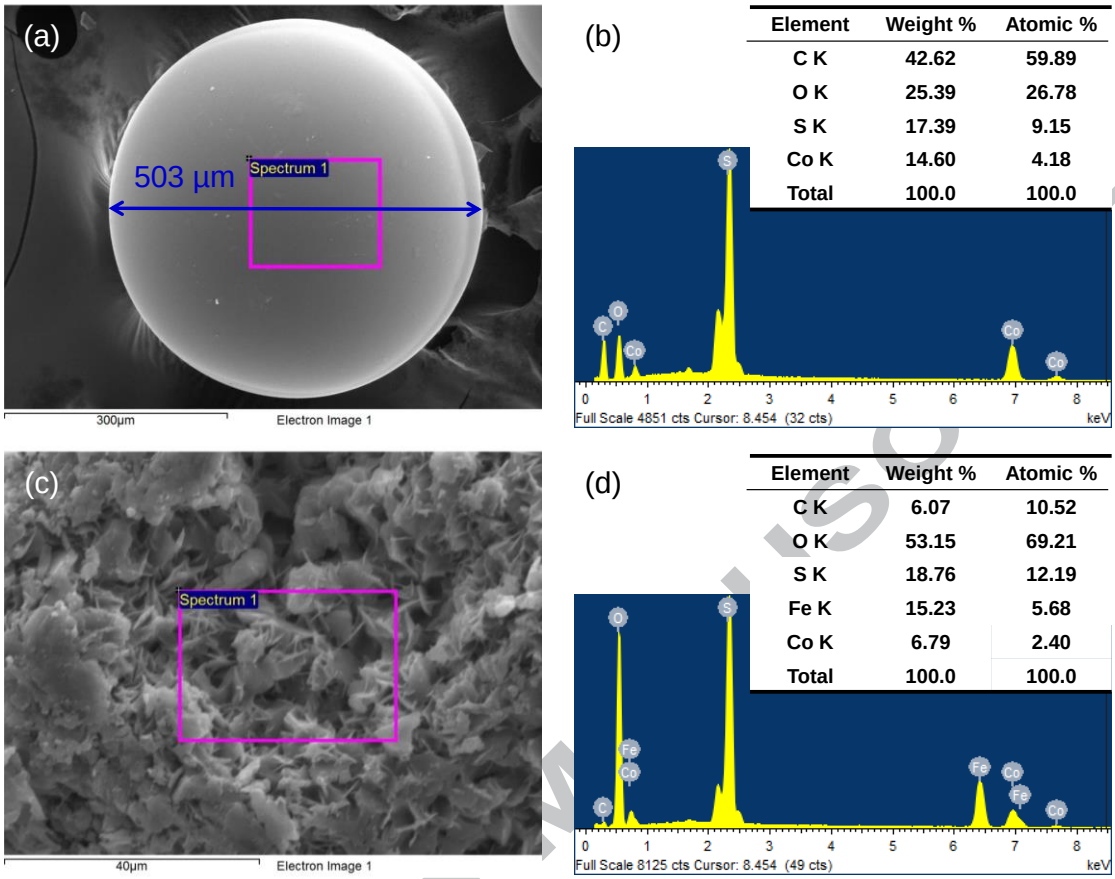

Figure 10

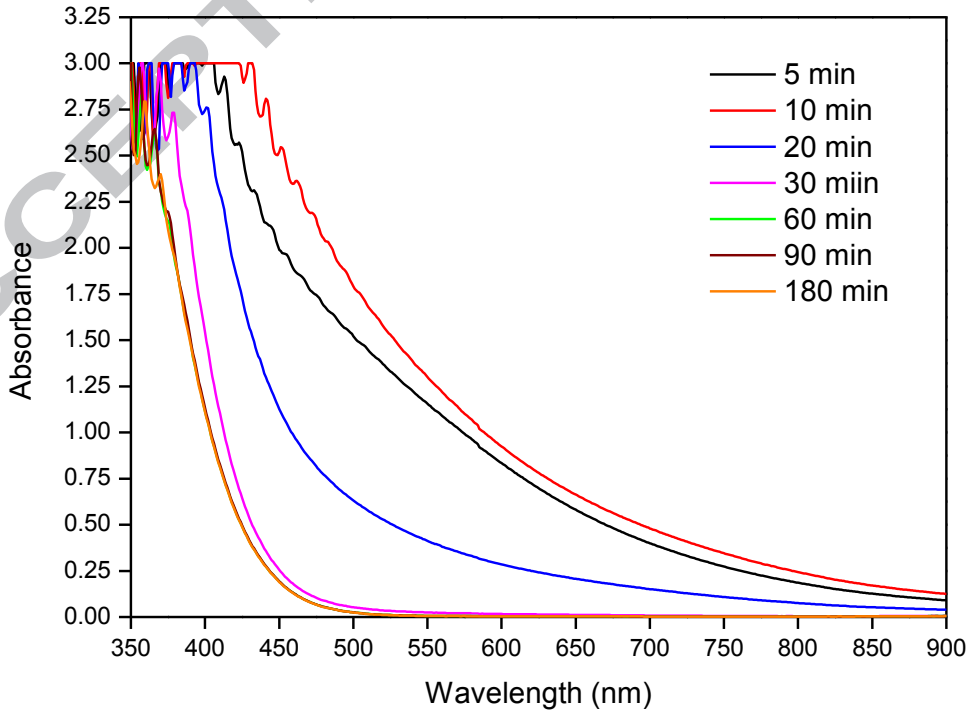

Figure 11

Bond	Bond length	Bond energy
C1–C2	1.5144	435.82
C3–C4	1.5140	436.95
C4–C5	1.5415	328.31
C5–C6	1.5460	316.20
C6–C7	1.5224	421.13
C8–S9	1.7822	372.14

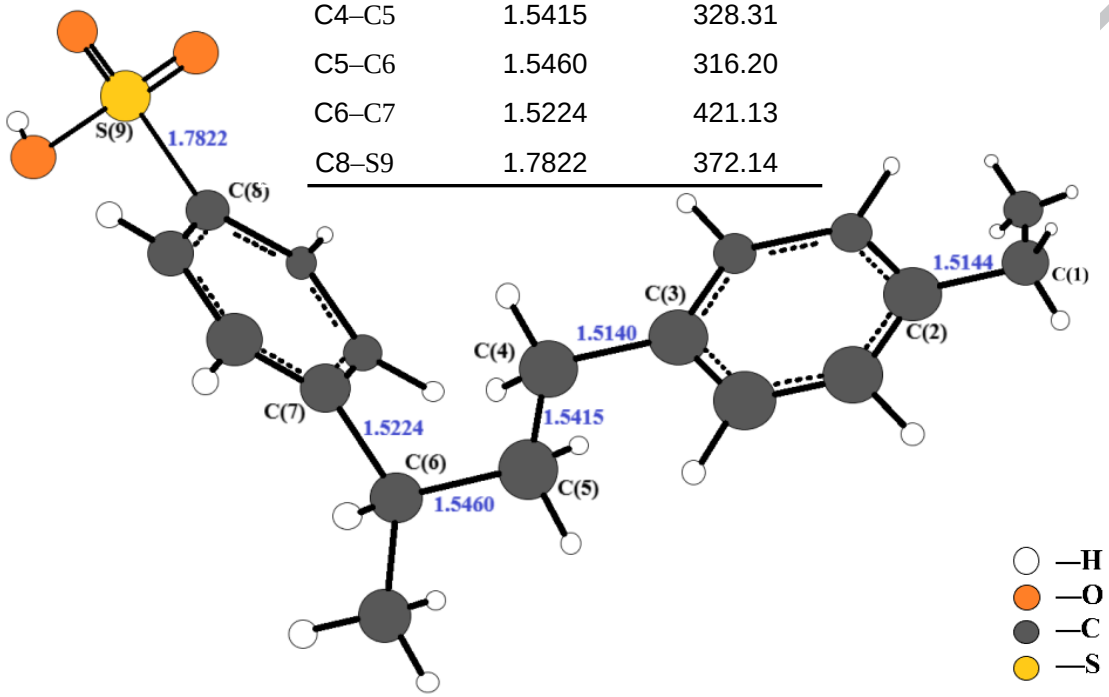

Figure 12

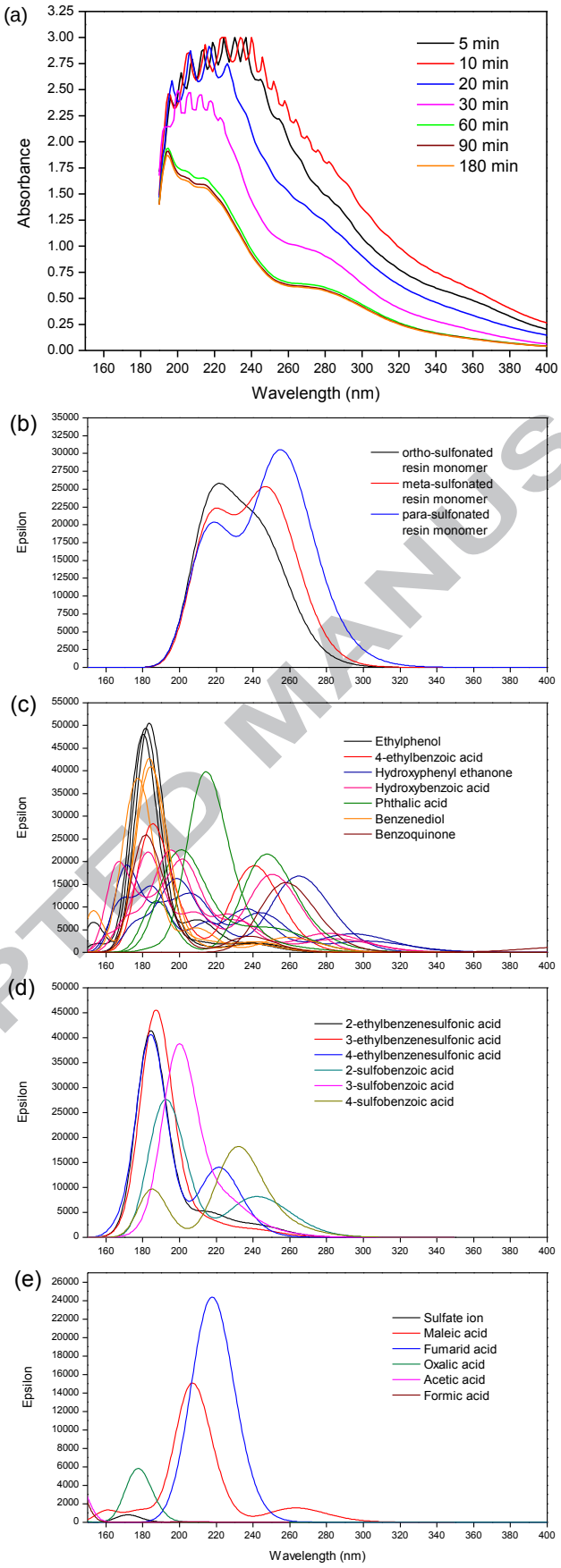

Figure 13

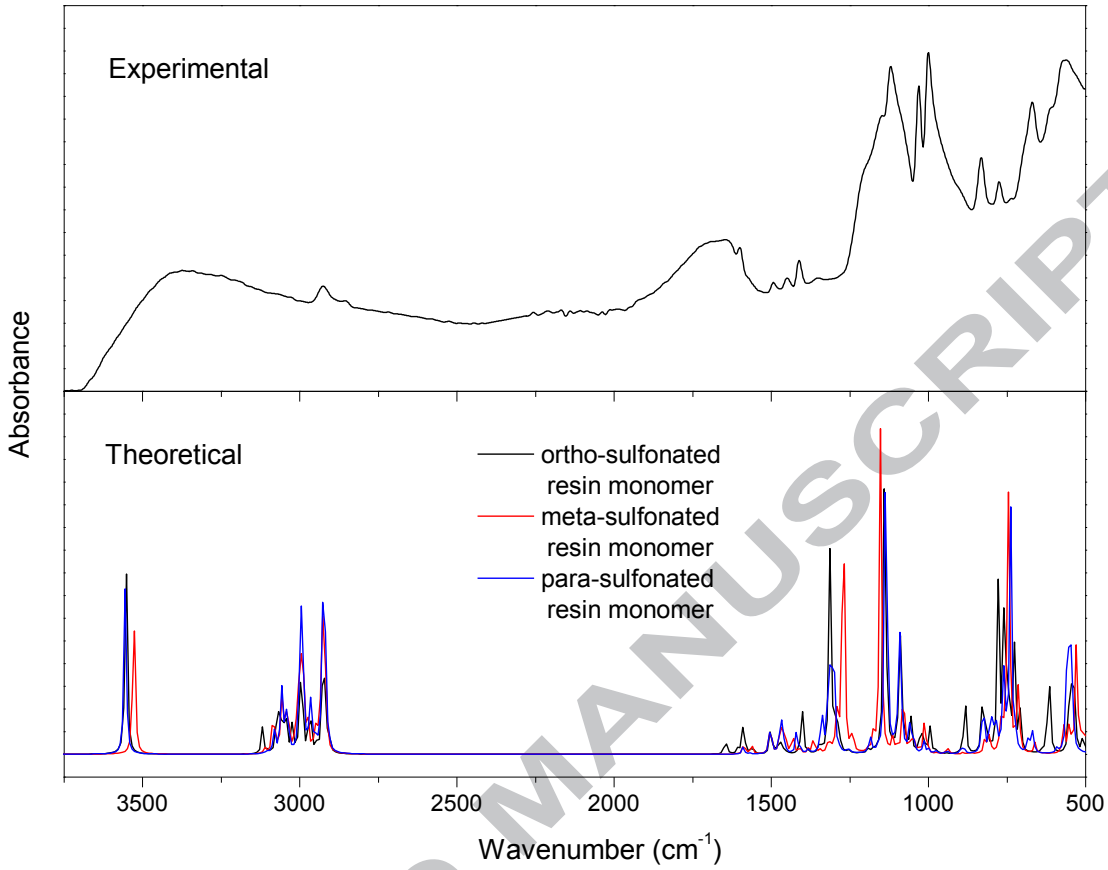

Figure 14

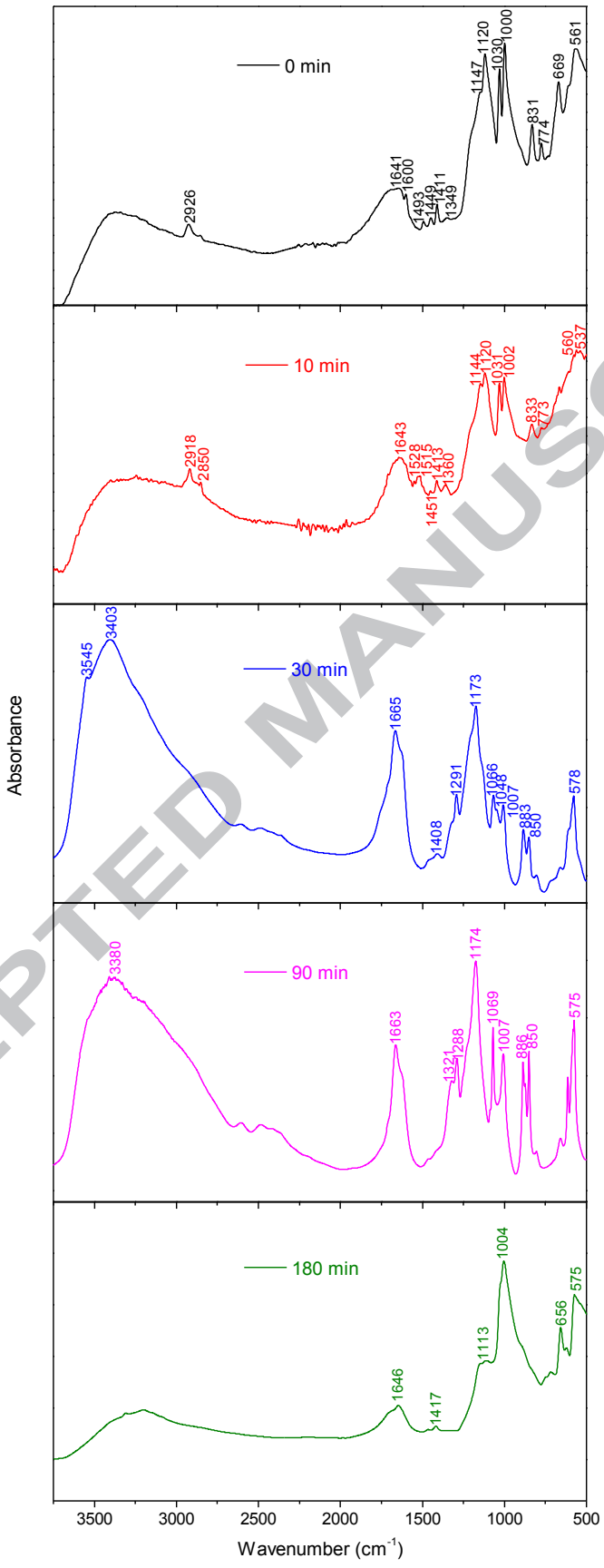

Table 1. The characteristics, performance and structure of the cationic resin.

Properties	ZG C NR 50
Physical form	Tan to brown translucent beads
Functional group	Sulfonic acid
Ionic form as shipped	H^+ (> 99.5%)
Degree of cross-linking (DVB)	8%
Total volume capacity	≥ 1.80 mmol/mL
Total ion exchange capacity	≥ 4.90 mmol/g
Moisture retention capacity	50–58%
Particle size	0.4–1.2 mm (≥ 95%)
Diameter <0.4 mm	≤ 1%
Whole beads	≥ 90%
Bulk density	0.75–0.85 g/mL
True density	1.18–1.24 g/mL
Maximum operating temperature	100 °C
Structure	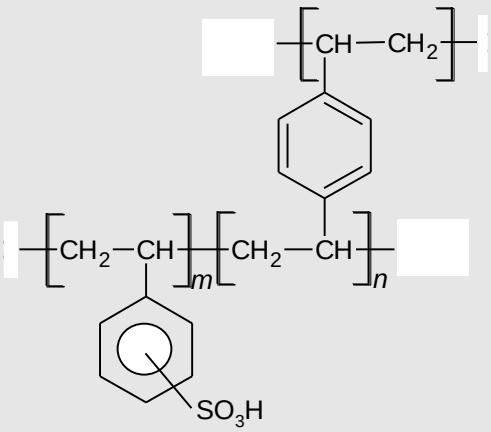

Table 2. Parameters of two-stage first-order kinetics for Fenton oxidation of cationic resins.

Operational parameters		k_1 (min^{-1})	R^2	k_2 (min^{-1})	R^2
Initial temperature (°C)	60	0.0064	0.9835	–	–
	75	0.0351	0.9317	-0.0027	0.8478

	90	–	–	-0.0218	0.9459
H_2O_2 dosage (mL)	100	–	–	-0.0027	0.8478
	150	–	–	-0.0173	0.9463
	200	–	–	-0.0507	0.9992
Fe^{2+} concentration (M)	0.1	–	–	-0.0165	0.9372
	0.3	–	–	-0.0507	0.9992
	0.5	–	–	-0.0152	0.9711
Initial pH	0.01	–	–	-0.0507	0.9992
	0.76	–	–	-0.0297	0.9698
	1.01	–	–	-0.0209	0.9638

Table 3. The experimental and calculated FTIR bands and tentative assignments of the fresh resin.

Experimental band positions (cm^{-1})	Calculated band positions (cm^{-1})	Assignments
2926	2926, 2992	C-H stretching
1641, 1600, 1493,	1674, 1653, 1564,	C-H in-plane vibration (benzene ring),
1449, 1411, 1349	1541, 1460, 1368	C=C stretching (benzene ring)
	1527, 1526	C-H in-plane vibration (carbon skeleton)
1147, 1120	1186, 1135, 1099	C-S and S=O wagging ($-SO_3H$ group)
1030, 1000	1037, 1033	C-H in-plane deformation (benzene ring)
831, 774	862, 777	C-H out-of-plane deformation (benzene ring)
669	640	benzene ring asymmetrical in-plane stretching
561	548	benzene ring symmetrical in-plane stretching

Table 4. The experimental FTIR bands and tentative assignments based on the DFT

calculations during decomposition process of resin.

Experimental band positions (cm^{-1})				Assignments
10 min	30 min	90 min	180 min	
	3545, 3403	3380		O-H stretching
2918, 2850				C-H stretching (benzene ring, -CH_2 and -CH_3 on the aliphatic group)
	1665	1663	1646	H_2O, C=C stretching (benzene ring), C-H in-plane vibration (benzene ring), C=O stretching
1643				H_2O, C=C stretching (benzene ring), O-H and benzene ring complex vibration
			1465, 1417	C=C stretching (benzene ring), C-H in-plane vibration (benzene ring), benzene ring in-plane deformation, C-H wagging
	1408			C-H in-plane vibration (benzene ring), C-H stretching (aliphatic group), O-H in-plane deformation (hydroxyl and carboxyl), C=C stretching (benzene ring)
1528, 1515, 1451, 1413				C=C stretching (benzene ring), C-H in-plane vibration (benzene ring), benzene ring in-plane deformation, C-H wagging

				(aliphatic group)
1360				benzene ring in-plane deformation, C-H wagging, C-O stretching (carboxylic acid)
		1321, 1288		C-H in-plane vibration (benzene ring), O-H in-plane wagging, C-H wagging (aliphatic group)
	1291			C-O stretching (carboxylic acid), C-H in-plane vibration (benzene ring), C-H wagging (aliphatic group), O-H in-plane wagging
	1173	1174		C-H in-plane vibration (benzene ring), C-O stretching or C-C stretching, O-H in-plane wagging (hydroxyl and carboxyl)
1144, 1120				$-SO_3H$, C-H in-plane vibration (benzene ring), O-H in-plane wagging (hydroxyl and carboxyl)
	1066, 1048	1069		C-H in-plane vibration (benzene ring), C-O stretching, O-H in-plane wagging
1031, 1002				C-H wagging (aliphatic group), C-C stretching, C-S stretching, benzene ring in-plane deformation
	1007	1007	1004	H wagging on the C=C bond, SO_4^{2-}
833, 773	883, 850	886, 850		C-H out-of-plane deformation

				(benzene ring)
560, 537	578	575	656, 575	SO_4^{2-}, O-H out-of-plane deformation (carboxylic acid), C-H out-of-plane deformation (benzene ring)

Highlights:

- Cationic resins were first dissolved and then degraded by Fenton oxidation.
- The oxidation of cationic resins followed the two-stage first-order kinetics.
- Complete dissolution of resin beads and 73% of weight reduction were observed.
- Reaction mechanism was deduced by experimental results and DFT calculations.

Graphical abstract: